

# Low temperature specific heat of the hole-doped $\text{Ba}_{0.6}\text{K}_{0.4}\text{Fe}_2\text{As}_2$ single crystals and electron-doped $\text{SmFeAsO}_{0.9}\text{F}_{0.1}$ samples

Gang Mu, Huiqian Luo, Zhaosheng Wang, Zhian Ren, Lei Shan, Cong Ren, and Hai-Hu Wen\*

National Laboratory for Superconductivity, Institute of Physics and Beijing National Laboratory for Condensed Matter Physics, Chinese Academy of Sciences, P.O. Box 603, Beijing 100190, People's Republic of China

Low temperature specific heat (SH) was measured on the FeAs-based superconducting single crystals  $\text{Ba}_{0.6}\text{K}_{0.4}\text{Fe}_2\text{As}_2$  and high pressure synthesized polycrystalline samples  $\text{SmFeAsO}_{0.9}\text{F}_{0.1}$ . It is found that the sharp SH anomaly  $\Delta C/T|_{T_c}$  in  $\text{Ba}_{0.6}\text{K}_{0.4}\text{Fe}_2\text{As}_2$  reaches an unexpected high value of 98 mJ/mol K<sup>2</sup>, about one order of magnitude larger than that of  $\text{SmFeAsO}_{0.9}\text{F}_{0.1}$  ( $6 \sim 8$  mJ/mol K<sup>2</sup>) samples, suggesting very high normal state quasiparticle density of states in FeAs-122 than in FeAs-1111. Furthermore, we found that the electronic SH coefficient  $\gamma_e(T)$  of  $\text{Ba}_{0.6}\text{K}_{0.4}\text{Fe}_2\text{As}_2$  is weakly temperature dependent and increases almost linearly with the magnetic field in low temperature region, which may indicate that the hole-doped FeAs-122 system contains a dominant component with a full superconducting gap, although we cannot rule out the possibility of a small component with anisotropic or nodal gap. A detailed analysis reveals that the  $\gamma_e(T)$  of  $\text{Ba}_{0.6}\text{K}_{0.4}\text{Fe}_2\text{As}_2$  cannot be fitted with a single gap of s-wave symmetry probably due to the multigap effect. These results indicate clear difference between the properties of the superconducting state of the hole-doped  $\text{Ba}_{0.6}\text{K}_{0.4}\text{Fe}_2\text{As}_2$  and the F-doped  $\text{LnFeAsO}$  ( $\text{Ln}$  = rare earth elements) systems, which we believe is originated from the complex Fermi surface structures in different systems.

PACS numbers: 74.20.Rp, 74.25.Bt, 65.40.Ba, 74.70.Dd

## I. INTRODUCTION

The discovery of high temperature superconductivity in the FeAs-based system has stimulated enormous interests in the fields of condensed matter physics and material sciences<sup>1</sup>. The superconductivity has not only been discovered in the electron-doped samples, but also in the hole-doped ones<sup>2,3</sup>. The central issues concerning the superconductivity mechanism are about the pairing symmetry and the magnitude of the superconducting gap. The experimental results obtained so far are, however, highly controversial. The low temperature specific heat (SH) measurements in the F-doped  $\text{LaFeAsO}$  samples revealed a nonlinear magnetic field dependence of the SH coefficient  $\gamma_e$ , which was attributed to the presence of a nodal gap<sup>4</sup>. This was later supported by many other measurements based on  $\mu\text{SR}$ <sup>5,6,7</sup>, NMR<sup>8,9,10</sup>, magnetic penetration<sup>11</sup> and point contact Andreev spectrum (PCAS)<sup>12</sup>. On the other hand, the PCAS on the F-doped  $\text{SmFeAsO}$  indicated a feature of s-wave gap<sup>13</sup>, some measurements<sup>14,15,16,17</sup> also gave support to this conclusion. It is important to note that most of the conclusions drawn for a nodal gap were obtained on the electron-doped  $\text{LnFeAsO}$  samples (abbreviated as FeAs-1111,  $\text{Ln}$  stands for the rare earth elements) which are characterized by a low charge carrier density and thus low superfluid density<sup>18</sup>. For the FeAs-1111 phase, it is very difficult to grow crystals with large sizes, therefore most of the measurements on the pairing symmetry so far were made on polycrystalline samples. This is much improved in the  $(\text{Ba},\text{Sr})_{1-x}\text{K}_x\text{Fe}_2\text{As}_2$  (denoted as FeAs-122) system since sizable single crystals can be achieved<sup>19</sup>. Preliminary data by angle resolved photo-emission spectroscopy (ARPES) on these crystals show two groups of superconducting gaps ( $\Delta_1 \approx 12$  meV,  $\Delta_2 \approx$

6 meV) all with s-wave symmetry<sup>20,21,22</sup>. It is known that the surface of this type of single crystals decay or reconstruct very quickly, this may give obstacles to get repeatable data when using the surface sensitive tools. Thus solid conclusions about the gap symmetry and magnitude from bulk measurements are highly desired.

Specific heat (SH) is one of the powerful tools to measure the bulk properties, especially about the quasiparticle density of states (DOS) at the Fermi level. By measuring the variation of the electronic SH versus temperature and magnetic field, one can essentially determine the feature of the gap symmetry. In this paper, for the first time, we report the detailed low temperature SH data on  $\text{Ba}_{0.6}\text{K}_{0.4}\text{Fe}_2\text{As}_2$  single crystals with  $T_c = 36.5$  K ( $90\%\rho_n$ ). We also present the SH data on a high pressure synthesized F-doped  $\text{SmFeAsO}$  sample for comparison. Our results reveal the existence of a dominant component with a full superconducting gap in  $\text{Ba}_{0.6}\text{K}_{0.4}\text{Fe}_2\text{As}_2$ , although we could not rule out the possibility that there might be small component of superfluid with the nodal gap. Therefore the FeAs-122 is very different from the case in the F-doped  $\text{LnFeAsO}$  where a nodal gap feature was discovered. Meanwhile we show the evidence of an unexpected large SH anomaly in the FeAs-122 superconductors, which is associated with the large DOS in the normal state. These two features indicate that there may be clear differences between the hole-doped FeAs-122 and the electron-doped FeAs-1111 phases. We argue that these differences are originated from the complex Fermi surface structures in different systems.<sup>23</sup> In the  $\text{Ba}_{0.6}\text{K}_{0.4}\text{Fe}_2\text{As}_2$  samples, the outer shell of the FSs surrounding  $\Gamma$  point takes most of the weight and exhibits a full gap. While in the F-doped  $\text{LnFeAsO}$ , the FSs near the M points contribute more weight to the superfluid and they have radical momentum dependence and nodes

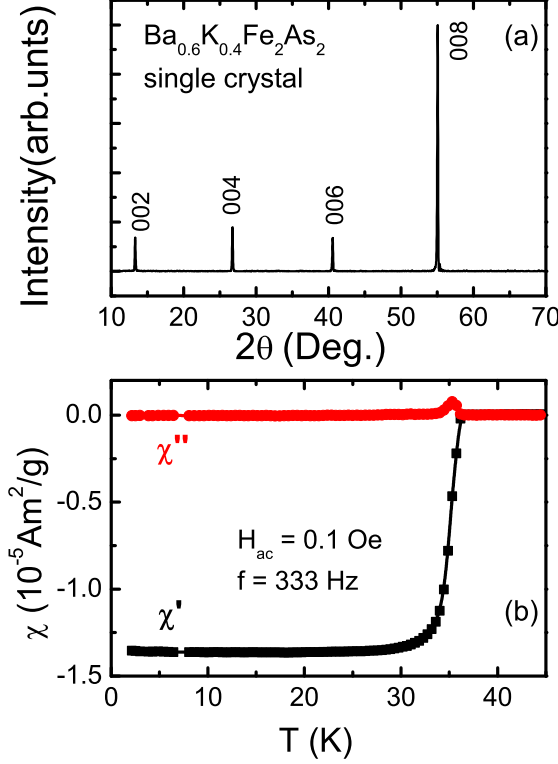


FIG. 1: (color online) (a) X-ray diffraction pattern measured for the single crystal of  $\text{Ba}_{0.6}\text{K}_{0.4}\text{Fe}_2\text{As}_2$  with  $T_c = 36.5$  K. Only sharp peaks along  $(00l)$  orientation were observed with the full-width-at-half-maximum (FWHM) of about  $0.10^\circ$ . (b) Temperature dependence of ac susceptibility for the same sample measured with  $H_{ac} = 1$  Oe and  $f = 333$  Hz. One can see a rather sharp transition with the onset transition temperature of about 36 K.

may be anticipated.

## II. SAMPLE PREPARATION AND CHARACTERIZATION

The superconducting single crystals of  $\text{Ba}_{1-x}\text{K}_x\text{Fe}_2\text{As}_2$  with  $T_c$  of about 36.5 K were grown by using FeAs as the self-flux<sup>19</sup>. The weighing and mixing procedures were performed in a glove box with a protective argon atmosphere. The mixed materials were placed in an alumina oxide crucible and sealed under vacuum in a quartz tube. The melting process was carried out at high temperatures of  $1000 \sim 1150^\circ\text{C}$ , and then a slowly cooling process was followed. The sample we chose for the SH measurement has the dimension of  $3.0 \times 1.5 \times 0.2 \text{ mm}^3$ . The potassium content was estimated to be about 40% from the EDX analysis<sup>19</sup>.

The X-ray diffraction (XRD) of the single crystals was carried out by a *Mac-Science* MXP18A-HF equipment

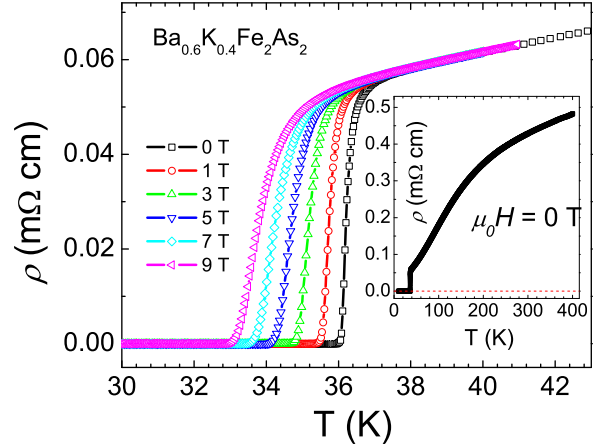


FIG. 2: (color online) Temperature dependence of the resistivity near superconducting transition for the  $\text{Ba}_{0.6}\text{K}_{0.4}\text{Fe}_2\text{As}_2$  sample at magnetic fields ranging from 0 to 9 T with  $H \parallel c$  axis. The inset shows the resistive curve under zero field up to 400 K.

with  $\theta - 2\theta$  scan. The ac susceptibility were measured based on an Oxford cryogenic system (Maglab-Exa-12). The resistivity and the specific heat were measured with a Quantum Design instrument physical property measurement system (PPMS) with the temperature down to 1.8 K and the magnetic field up to 9 T. The temperature stabilization was better than 0.1% and the resolution of the voltmeter was better than 10 nV. We employed the thermal relaxation technique to perform the specific heat measurements. To improve the resolution, we used a latest developed SH measuring frame from Quantum Design, which has negligible field dependence of the sensor of the thermometer on the chip as well as the thermal conductance of the thermal linking wires.

The crystal structure of sample  $\text{Ba}_{0.6}\text{K}_{0.4}\text{Fe}_2\text{As}_2$  with  $T_c = 36.5$  K was examined by XRD measurement with incident X-ray along the  $c$ -axis direction. The XRD pattern is shown in Fig. 1(a). It is clear that only sharp peaks along  $(00l)$  orientation can be observed, suggesting a high  $c$ -axis orientation. The full-width-at-half-maximum (FWHM) of the diffraction peaks were only about  $0.10^\circ$ , indicating a rather fine crystalline quality in the present sample. The diamagnetic transition measured with ac susceptibility technique is shown in Fig. 1(b). A rather sharp transition at about 36 K (onset) can be seen, which provides an evidence for the homogeneity of the superconducting properties of our sample.

In Fig. 2, we show the temperature dependence of the in-plane electrical resistivity near  $T_c$  at magnetic field up to 9 T with  $H \parallel c$  axis for the sample  $\text{Ba}_{0.6}\text{K}_{0.4}\text{Fe}_2\text{As}_2$ . The onset transition temperature ( $90\%\rho_n$ ) is determined to be about 36.5 K under zero field. And a rather narrow transition width ( $\Delta T_c \sim 1$

K) can be observed when the magnetic field is lower than 3 T, which also suggests the high quality of the present sample. By applying a magnetic field the middle transition point ( $50\%\rho_n$ ) shifts to lower temperatures slowly with a slope  $-d\mu_0 H_{c2}(T)/dT|_{T_c} \approx 4.1$  T/K. Using the Werthamer-Helfand-Hohenberg relation<sup>24</sup>  $\mu_0 H_{c2}(0) = -0.69d\mu_0 H_{c2}(T)/dT|_{T_c} T_c$ , we get the upper critical field  $\mu_0 H_{c2}(0) \approx 100$  T ( $H \parallel c$ ). The inset of Fig. 2 shows temperature dependence of the resistivity in a wide temperature regime up to 400 K at zero field. One can see that the  $\rho - T$  curve exhibits a continued curvature in the normal state up to 400 K.

The fluorine doped SmFeAsO superconducting samples were prepared by a high pressure synthesis method. The details about the synthesis were reported previously.<sup>25</sup> As shown in Fig. 3, the ac susceptibility data (measured using an ac amplitude of 0.1 Oe) exhibits a sharp magnetic transition. The width defined between the 10% and 90% cuts of the transition is below 2 K, with the middle transition point at 51.5 K, indicating a very good quality of the superconducting phase. The inset shows a scanning electron microscope picture of the sample. Compared with the samples synthesized at ambient pressures, the samples studied here are much more compact. A rough estimate on the diamagnetic signal indicates that the superconducting volume is close to 100 %. The relatively sharp superconducting transition and the large fraction of the superconducting volume validate the specific heat measurements and the data analysis in this paper.

### III. ANALYSIS TO THE SPECIFIC HEAT DATA OF $\text{Ba}_{0.6}\text{K}_{0.4}\text{Fe}_2\text{As}_2$

In the main panel of Fig. 4 we show the raw data of SH coefficient  $\gamma = C/T$  vs  $T$  for  $\text{Ba}_{0.6}\text{K}_{0.4}\text{Fe}_2\text{As}_2$  sample at 0 T and 9 T. Multiple complicated contributions to the SH data emerged in the low-T region when a magnetic field was applied, so we only show the data above 4.3 K under magnetic fields, and the data at zero field was shown down to about 1.8 K. Clear and sharp superconducting anomalies can be seen near  $T_c$  from the raw data. The SH anomaly  $\Delta C/T|_{T_c}$  at zero field was determined to be about 98 mJ/mol K<sup>2</sup>, indicated by the vertical short blue line in the inset of Fig. 4. This is remarkably different from the case in the FeAs-1111 phase, where only a very small SH anomaly (less than 8 mJ/mol K<sup>2</sup>) was observed in the raw data<sup>4,26,27</sup>. In section V, we will display the SH data of a high-pressure synthesized sample  $\text{SmFeAsO}_{0.9}\text{F}_{0.1}$ , where the SH anomaly near  $T_c$  reaches only 6~8 mJ/mol K<sup>2</sup>. Therefore the large value of  $\Delta C/T|_{T_c}$  in  $\text{Ba}_{0.6}\text{K}_{0.4}\text{Fe}_2\text{As}_2$  is an intrinsic property, it may be associated with the high quasiparticle DOS in the normal state, which will be further addressed later. A magnetic field of 9 T shifts the SH anomaly down for only 1.5 K and suppresses the anomaly clearly. This is consistent very well with the resistive measurements which

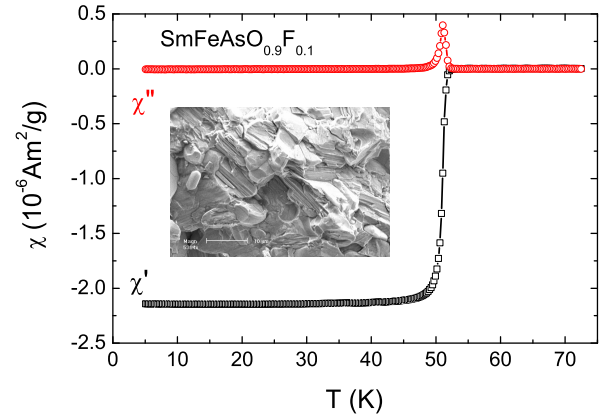


FIG. 3: (color online) Temperature dependence of the ac susceptibility of the high pressure synthesized bulk sample  $\text{SmFeAsO}_{0.9}\text{F}_{0.1}$  measured with an ac field of 0.1 Oe and frequency of 333 Hz. A very sharp superconducting transition is obvious. A rough estimate on the magnetic signal indicates that the superconducting volume is close to 100 %. The inset shows a scanning electron microscope picture of the sample. The grains with plate-like shape are highly compacted together.

indicate that the upper critical field is very high in this system.<sup>28</sup> Below about 10 K, a clear flattening feature of  $C/T$  can be seen in Fig. 4, which may imply the weak excitation of quasiparticles.

The raw data in the low temperature region at different fields are plotted as  $C/T$  vs  $T^2$  in Fig. 5(a). A slight curvature was detected in the region from 4.3 K to 11 K on the plot of  $C/T$  vs.  $T^2$ , which was attributed to the electron contribution of the superconducting state and the quintic term of the phonon contribution. This brought in enormous difficulties when treating the data because it gave too many fitting parameters. Therefore we first analyze the data below 6 K at zero field, where the two terms mentioned above remain negligible. Consequently the zero field data below 6 K can be represented by the following equation:

$$C(T, H = 0) = \gamma_0 T + \beta T^3 + C_{Sch}(T, H = 0), \quad (1)$$

where the three terms represent the contributions of the residual electronic SH, the phonon and the magnetic impurity (the so-called Schottky anomaly), respectively. The Schottky anomaly is generally induced by lifting the degeneracy of the states of the paramagnetic spins in the magnetic impurities<sup>29,30</sup> and is given by

$$C_{Sch}(T, H) = n \left( \frac{g\mu_B H_{eff}}{k_B T} \right)^2 \frac{e^{\frac{g\mu_B H_{eff}}{k_B T}}}{(1 + e^{\frac{g\mu_B H_{eff}}{k_B T}})^2}, \quad (2)$$

where  $g$  is the Landé factor,  $\mu_B$  is the Bohr magneton,  $H_{eff} = \sqrt{H^2 + H_0^2}$  is the effective magnetic field which

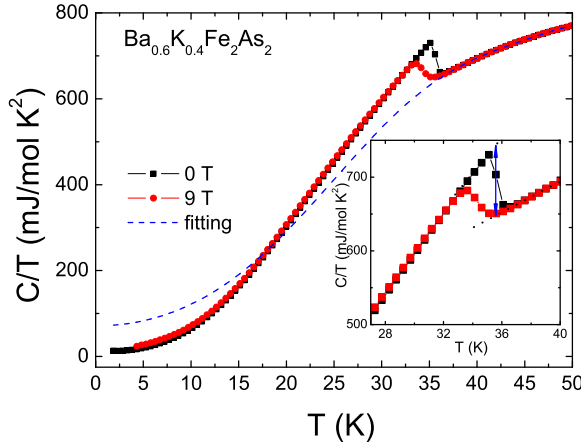


FIG. 4: (color online) Raw data of SH coefficient  $\gamma = C/T$  vs  $T$  for  $\text{Ba}_{0.6}\text{K}_{0.4}\text{Fe}_2\text{As}_2$  sample are shown in the main frame. The dashed line shows the normal state SH obtained from fitting to Eq. (6). The inset shows an enlarged view of the data  $\gamma = C/T$  near  $T_c$ . The sharp SH anomaly  $\Delta C/T|_{T_c}$  is indicated by the arrowed blue short line with a magnitude of about 98 mJ/mol K<sup>2</sup>.

evolves into  $H_{eff} = H_0$ , the crystal field at zero external field, and  $n$  is the concentration of paramagnetic centers. The obtained fitting parameters  $\gamma_0 \approx 7.7$  mJ/mol K<sup>2</sup> and  $\beta \approx 0.473$  mJ/mol K<sup>4</sup> are very close to the values obtained by simply drawing a linear line below 6 K as shown by the dot-dashed line in Fig. 5(a). The values of  $\gamma_0$  and  $\beta$  are then fixed when fitting the zero field data up to 11 K, where all the terms must be taken into account:

$$C(T, H = 0) = \gamma_0 T + [\beta T^3 + \eta T^5] + C_{es} + C_{Sch}(T, H = 0), \quad (3)$$

where  $\eta$  is the quintic term coefficient of the phonon SH and  $C_{es} = D \times e^{-\Delta(0)/k_B T} / T^{1.5}$  is the superconducting electron contribution based on an s-wave scenario, with  $\Delta(0)$  the superconducting gap at 0 K. By fitting the data at zero field using Eq. (3), we obtained  $\eta \approx 0.00034$  mJ/mol K<sup>6</sup> and  $\Delta(0) \approx 5.99 \pm 0.03$  meV. As for the data under finite fields, a magnetic field induced term  $\gamma(H)$  arises and the total SH can be written as

$$C(T, H) = [\gamma_0 + \gamma(H)]T + [\beta T^3 + \eta T^5] + C_{es} + C_{Sch}(T, H). \quad (4)$$

It is quite rational to fix  $\gamma_0$ ,  $\beta$ , and  $\eta$  as the values obtained from analyzing the data at zero field. And the superconducting gap under magnetic fields was restricted using the relation<sup>31</sup>  $\Delta(H) = \Delta(0) \sqrt{1 - H/H_{c2}}$  assuming a field induced pair breaking effect. In this way the number of the fitting parameters were reduced remarkably and creditable results can be obtained.

We should however, note that in treating the data with above equations, we assumed a dominant contribution of superfluid with s-wave symmetry. This does not mean

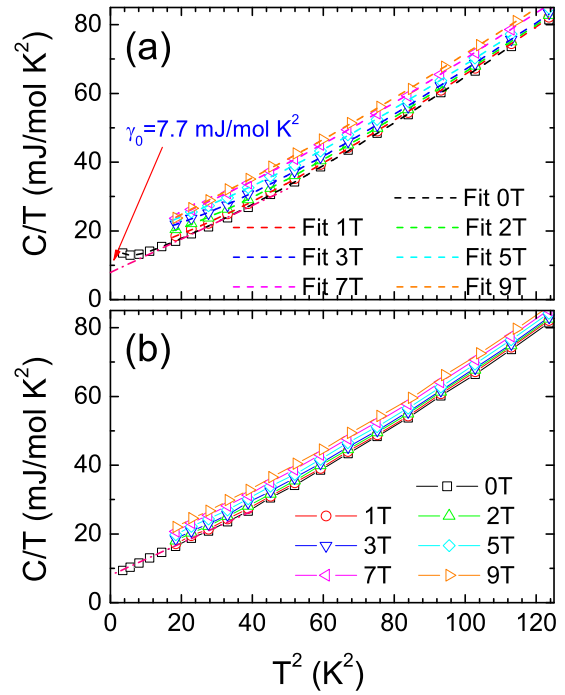


FIG. 5: (color online) Temperature and magnetic field dependence of specific heat in  $C/T$  vs  $T^2$  plot in the low temperature range. (a) Raw data before removing the Schottky anomaly. The dashed lines represent the theoretical fit (see text) containing all terms in Eq. (4). (b) Replot of the data after the Schottky anomaly was subtracted. The dot-dashed line represents an extension of the zero field data to  $T = 0$  K giving a residual value  $\gamma_0 = 7.7$  mJ/mol K<sup>2</sup> (see text).

that we can rule out the possibility of some small components of superfluid with a nodal gap. This is because a component with nodes will contribute a power law term to the specific heat in the low temperature limit, which cannot be easily separated from the combination of the residual term  $\gamma_0 T$  and the phonon term  $\beta T^3$ . However, from the field dependence of the specific heat, we confirm that this possible small component with nodes takes only a very small part of the total condensate, since the specific heat coefficient increases almost linearly with the magnetic field, as predicted for an s-wave gap.

Fig. 5(b) shows the data after removing the Schottky anomaly from the total SH. The obtained field induced term  $\gamma(H)$  are shown in Fig. 6 (will be discussed later) and the fitting parameters related to the terms  $C_{es}$  and  $C_{Sch}$  are shown in Table I. The obtained residual term  $\gamma_0 \approx 7.7$  mJ/mol K<sup>2</sup> accounts for about 11% of the total electron contribution (will be discussed later), indicating a superconducting volume fraction of about 89% in our sample. Using the obtained value of  $\beta$  and the relation  $\Theta_D = (12\pi^4 k_B N_A Z / 5\beta)^{1/3}$ , where  $N_A = 6.02 \times 10^{23}$  mol<sup>-1</sup> is the Avogadro constant,  $Z = 5$  is the number of

TABLE I: Fitting parameters ( $\Delta$  is calculated through  $\Delta(H) = \Delta(0)\sqrt{1 - H/H_{c2}}$ ,  $H_0$  is fixed with the value from the fitting to zero-field data).

$\mu_0 H$ (T)	$D$ (mJ K <sup>0.5</sup> /mol)	$\Delta$ (meV)	$n$ (mJ/mol K)	$\mu_0 H_0$ (T)	$g$
0.0	$2.11 \times 10^6$	5.99	20.95	1.70	2.75
1.0	$2.07 \times 10^6$	5.96	31.08	1.70	3.18
2.0	$1.93 \times 10^6$	5.93	35.76	1.70	3.26
3.0	$1.82 \times 10^6$	5.90	36.22	1.70	3.38
5.0	$1.63 \times 10^6$	5.84	36.11	1.70	3.24
7.0	$1.57 \times 10^6$	5.78	36.71	1.70	3.11
9.0	$1.43 \times 10^6$	5.72	35.98	1.70	3.22

atoms in one unit cell, we get the Debye temperature  $\Theta_D \approx 274$  K. This value is close to that found in the LaFeAsO<sub>0.9</sub>F<sub>0.1- $\delta$</sub>  system<sup>4</sup>.

#### IV. A DOMINANT COMPONENT OF SUPERFLUID WITH S-WAVE SYMMETRY AND VERY HIGH DOS IN $\text{Ba}_{0.6}\text{K}_{0.4}\text{Fe}_2\text{As}_2$

The field-induced change of the electron SH coefficient  $\gamma(H)$  was obtained from fitting and plotted in Fig. 6. It can be seen clearly that  $\gamma(H)$  increases almost linearly with the magnetic field in the temperature region up to 11 K. A linear fit with the slope of about 0.633 mJ/mol K<sup>2</sup> T to the zero temperature data is revealed by the blue solid line in this figure. It is clear that the  $\gamma(H)$ – $H$  curve roughly displays a linear behavior at all temperatures below 11 K. This linear behavior is actually anticipated by the theoretical prediction for superconductors with a full gap<sup>32</sup>, in which  $\gamma(H)$  is mainly contributed by the localized quasiparticle DOS within vortex cores. So it seems that the superconductivity in the FeAs-122 phase is primarily dominated by a full-gap state around the hole-like Fermi surface at  $\Gamma$  point and the field-induced quasiparticle DOS are mainly contributed by the vortex cores. This is in sharp contrast with the results in cuprates<sup>33,34,35,36</sup> and the LaFeAsO<sub>0.9</sub>F<sub>0.1- $\delta$</sub>  system<sup>4</sup> where a  $\gamma(H) \propto \sqrt{H}$  relation was observed and attributed to the Doppler shift of the nodal quasiparticle spectrum. The curve plotted using the relation  $\gamma(H) = A\sqrt{H}$  is also presented in Fig. 6. It is obvious that this curve fails to fit our data. We have also attempted to fit the data by mixing linear and square root behavior as revealed by the navy-blue solid line in Fig. 6. One can see that this curve can also roughly describe the behavior of our data. So there is the possibility for the presence of a d-wave gap at different positions of the Fermi surface.

In order to further confirm this point, we analyzed the SH data in finite temperature region in the mixed state. It is known that the quasiparticle excitations in superconductors with different gap symmetry can be obviously distinct. In s-wave superconductors, the inner-core states dominate the quasiparticle excitations, and consequently

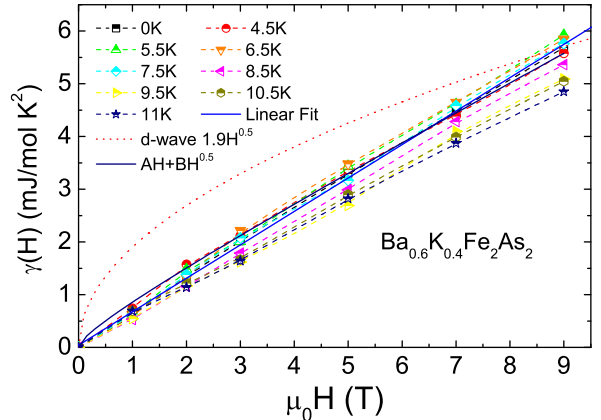


FIG. 6: (color online) Field dependence of the field-induced term  $\gamma(H)$  at temperatures ranging from 4.5 K to 11.1 K, and that at  $T = 0$  K obtained from fitting (see text). The dashed lines for different temperatures are guides for the eyes. The blue solid, red dotted, and navy-blue solid line are the linear fit to the zero temperature data, the fit to the d-wave prediction  $\gamma(H) = A\sqrt{H}$ , and the fit by mixing the above two components, respectively.

a simple scaling law  $C_{core}/T^3 \approx (\gamma_n/H_{c2(0)}) \times (T/\sqrt{H})^{-2}$  for the fully gapped superconductors is expected. While for a gap with line nodes, the excitation spectrum is dominated by the extended quasiparticles outside the vortex cores. And the so-called Simon-Lee scaling law<sup>37</sup>  $C_{vol}/(T\sqrt{H}) = f(T/\sqrt{H})$  should be obeyed. A simple analysis similar to that has been done in our previous work<sup>38</sup> shows that for the superconductor with an s-wave symmetry,  $C_{cal-s} = [(C(H) - C_{Sch}(H)) - (C(H = 0) - C_{Sch}(H = 0))]/T^3 \approx C_{core}/T^3$ , considering the fact that the phonon SH is independent on the magnetic field. In other words, the defined term  $C_{cal-s}$  should scale with  $T/\sqrt{H}$  with the prefactor  $\gamma_n/H_{c2(0)}$ . Similarly for the d-wave symmetry we have known<sup>36,38</sup> that  $C_{cal-d} = [(C(H) - C_{Sch}(H)) - (C(H = 0) - C_{Sch}(H = 0))]/T\sqrt{H} = C_{vol}/T\sqrt{H} - \alpha T/\sqrt{H}$ , where  $\alpha$  is the electron SH coefficient at zero field for a d-wave superconductor, should also scale with  $T/\sqrt{H}$ . The scaling result of the field-induced term in the mixed state with the s-wave condition is presented in Fig. 7(a). One can see that all the data at different magnetic fields can be scaled roughly to one straight line, which reflects the theoretical curve  $C_{cal-s} = 0.633 \times (T/\sqrt{H})^{-2}$ . Naturally, this prefactor  $\gamma_n/H_{c2(0)} = 0.633 \text{ mJ}/(\text{mol K}^2 \text{ T})$  is consistent with the magnitude of the slope of the blue line in Fig. 6. Using the value of  $H_{c2(0)} \approx 100$  T, we can estimate the normal state electron SH coefficient  $\gamma_n$  of about 63.3 mJ/mol K<sup>2</sup>, a rather large value compared with the F-doped LaFeAsO system<sup>4</sup> and SmFeAsO system which will be revealed in the next section. Fig. 7(b) shows the scaling by follow-

ing the d-wave scheme. It is clear that the s-wave scaling is much better than that of the d-wave case. This again indicates that the superconducting state in this FeAs-112 phase is dominated by an s-wave symmetry gap and the field-induced quasiparticle DOS are mainly contributed by the vortex cores. And the slight departure of the scaling in Fig. 7(a) may suggest that small amount of d-wave components exist in the superconducting state.

Using the value of  $\gamma_n \approx 63.3$  mJ/mol K<sup>2</sup>, we get the ratio  $\Delta C_e/\gamma_n T|_{T_c} \approx 1.55$  being very close to the weak-coupling BCS value 1.43. Considering the electron re-normalization effect, the electron SH coefficient of a metal can be written as

$$\gamma_n = \frac{2\pi^2}{3} N(E_F) k_B^2 (1 + \lambda), \quad (5)$$

where  $N(E_F)$  is the DOS at the Fermi surface and  $\lambda$  reflects the coupling strength. The fact that the electron-phonon coupling strength is weak in present system indicates that the large value of  $\gamma_n$  is not due to the enhanced effective mass but originates from the high normal state quasiparticle DOS. Comparing with the  $\gamma_n$  obtained for the F-doped LaFeAsO system<sup>4</sup> (about 5-6 mJ/mol-Fe K<sup>2</sup>), the  $N(E_F)$  in hole-doped FeAs-122 phase may be 5-10 times higher than that in the electron-doped FeAs-1111 phase. Although the band structure calculations gave a relatively larger  $\gamma_n$  in FeAs-122<sup>39,40,41,42,43</sup> than in FeAs-1111, the predicted values are however hardly beyond 15 mJ/mol K<sup>2</sup> which is much below the experimental value found here  $\gamma_n \approx 63.3$  mJ/mol K<sup>2</sup>. An appropriate explanation to this large discrepancy is highly desired from the theoretical side.

In the FeAs-122 superconductors, it is challenging to measure the normal state SH below  $T_c$  due to the very high  $H_{c2}$ . In order to have a comprehensive understanding to the normal state SH, we have attempted to fit the normal state SH above  $T_c$  using a polynomial function:

$$C_n = (\gamma_0 + \gamma_n)T + \beta_3 T^3 + \beta_5 T^5 + \beta_7 T^7 + \beta_9 T^9 + \beta_{11} T^{11}, \quad (6)$$

where we took the values obtained already  $\gamma_0 = 7.7$  mJ/mol K<sup>2</sup>,  $\gamma_n = 63.3$  mJ/mol K<sup>2</sup>, and  $\beta_3 = 0.473$  mJ/mol K<sup>4</sup>. Other fitting parameters,  $\beta_5$ ,  $\beta_7$ ,  $\beta_9$ , and  $\beta_{11}$ , were left free in the fitting process, yielding the values of  $3.72 \times 10^{-4}$  mJ/mol K<sup>6</sup>,  $-5.32 \times 10^{-7}$  mJ/mol K<sup>8</sup>,  $2.13 \times 10^{-10}$  mJ/mol K<sup>10</sup>, and  $-2.90 \times 10^{-14}$  mJ/mol K<sup>12</sup>, respectively. It's worth to note that the value of  $\beta_5$  is very close to the value of  $\eta$  obtained before. The fitting result of the normal state SH is displayed by the blue dashed line in the main frame of Fig. 4. The data after subtracting the normal state SH is presented in the main frame of Fig. 8. It was found that the entropy-conserving law was satisfied naturally confirming the validity of our fitting, as shown in the inset of Fig. 8. A clear flattening of  $\gamma_e - \gamma_n$  in the temperature region below 7 K is observed indicating a fully gapped superconducting state. Moreover, a hump is clearly seen in the middle temperature region. We attempted to fit the data using the BCS

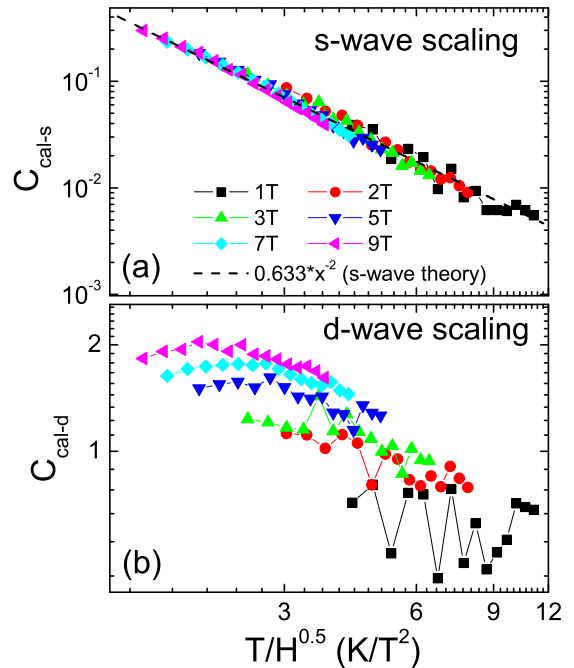


FIG. 7: (color online) (a) Scaling of the data according to the s-wave scenario (symbols)  $C_{cal-s} = [(C(H) - C_{Sch}(H)) - (C(H = 0) - C_{Sch}(H = 0))] / T^3$  vs.  $T/\sqrt{H}$ , the dashed line represents the theoretical expression. (b) Scaling of the data (symbols) based on d-wave prediction  $C_{cal-d} = [(C(H) - C_{Sch}(H)) - (C(H = 0) - C_{Sch}(H = 0))] / T\sqrt{H}$  vs.  $T/\sqrt{H}$ . No good scaling can be found for the d-wave case.

formula:

$$\gamma_e = \frac{4N(E_F)}{k_B T^3} \int_0^{+\infty} \int_0^{2\pi} \frac{e^{\zeta/k_B T}}{(1 + e^{\zeta/k_B T})^2} (\varepsilon^2 + \Delta^2(\theta, T) - \frac{T}{2} \frac{d\Delta^2(\theta, T)}{dT}) d\theta d\varepsilon, \quad (7)$$

where  $\zeta = \sqrt{\varepsilon^2 + \Delta^2(T, \theta)}$  and  $\Delta(T, \theta) = \Delta_0(T)$  for the s-wave symmetry. The red dashed line in the main frame presented the fitting result. One can see that the fitting curve with a gap value of about 6 meV matched our data below 13 K perfectly, but failed to describe the hump feature in the middle temperature region. This hump may be attributed to the multi-gap effect which seems to appear in the FeAs-based superconductors, and small components with d-wave gap may appear in some positions of the Fermi surface. But at this moment we cannot exclude the possibility that the hump is induced by the limited uncertainty in getting the normal state phonon contribution. Nevertheless, the fine fitting in wide temperature region strongly suggests that the dominant part of the superconducting condensate is induced by a full gap with the magnitude of about 6 meV. Our results here seem to be consistent with the ARPES data, both in symmetry

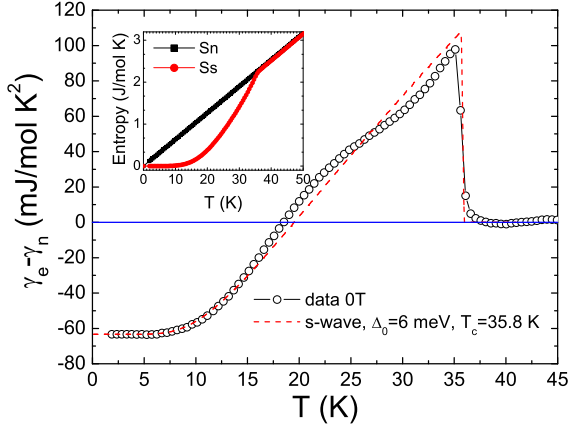


FIG. 8: (color online) Temperature dependence of the electronic SH contribution (with the normal state part subtracted) is shown in the main frame. A sharp SH anomaly can be seen here. A hump is clearly seen in the middle temperature region. The red dashed line is a theoretical curve based on the BCS expression with an s-wave gap of 6 meV. The inset shows the entropy of the superconducting state (red circle symbols) and the normal state (dark square symbols).

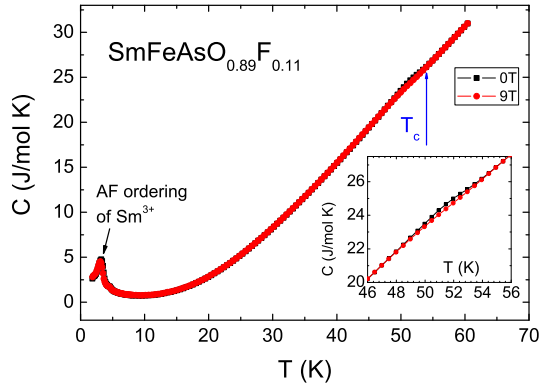


FIG. 9: (color online) Temperature dependence of SH for the electron-doped  $\text{SmFeAsO}_{0.9}\text{F}_{0.1}$  under 0 T and 9 T is shown in the main frame. The arrowed blue line denotes the superconducting transition temperature. A clear peak can be observed at about 3.2 K under both fields. This peak was observed previously and attributed to the anti-ferromagnetic ordering of the  $\text{Sm}^{3+}$  ions. The inset shows an enlarged view of the main frame near  $T_c$ .

and the small gap<sup>20,21,22</sup>. But we have not found a large gap of 12 meV. This discrepancy may be induced by the different ways in determining the gap. Future works are certainly required to reconcile all these distinct results.

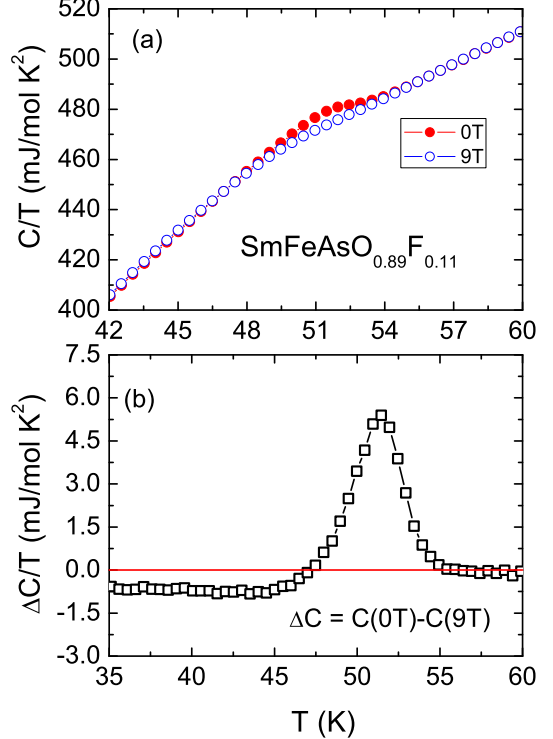


FIG. 10: (color online) (a) Specific heat data of the sample  $\text{SmFeAsO}_{0.9}\text{F}_{0.1}$  under two different fields 0 T and 9 T, plotted as  $C/T$  vs  $T$  close to  $T_c$ . (b)  $(C(0\text{T})-C(9\text{T}))/T$  vs  $T$  for the same sample. One can see a clear specific heat peak near the onset temperature of the ac susceptibility curve.

## V. SPECIFIC HEAT OF ELECTRON-DOPED $\text{SmFeAsO}_{0.9}\text{F}_{0.1}$

We have also investigated the low temperature SH of the electron-doped  $\text{SmFeAsO}_{0.9}\text{F}_{0.1}$  polycrystalline sample with high quality prepared using a high pressure (HP) synthesis method<sup>25</sup>. In the main frame of Fig. 9, we show the temperature dependence of the SH in  $\text{SmFeAsO}_{0.9}\text{F}_{0.1}$  at 0 T and 9 T. The clear peak in the low temperature regime (around 3.2 K) was attributed to the anti-ferromagnetic ordering of  $\text{Sm}^{3+}$  ions in this system<sup>27</sup>. The SH anomaly near  $T_c$  denoted by the arrowed blue line is quite unobtrusive, even in the enlarged view as shown in the inset of Fig. 9, indicating a rather low DOS or superfluid density in the present system.

The SH data of  $\text{SmFeAsO}_{0.9}\text{F}_{0.1}$  near  $T_c$  under two different magnetic fields 0 T and 9 T are plotted as  $C/T$  vs  $T$  in Fig. 10(a). The SH anomaly can be observed and it has a width of about 3 K, which is quite narrow comparing with the  $T_c$ . This relatively narrow SH anomaly strongly suggests that the small magnitude of the SH anomaly is an intrinsic feature, not because the sample is a polycrystalline one. It is clear that the be-

havior in this figure is in sharp contrast with that of the hole-doped  $\text{Ba}_{0.6}\text{K}_{0.4}\text{Fe}_2\text{As}_2$  where a sharp and huge peak has been detected, as shown in the inset of Fig. 4. In Fig. 10(b) we show the discrepancy of the data in the two curves of Fig. 10(a). A peak due to superconducting phase transition shows up clearly. The behavior observed here is quite similar to that reported by other groups<sup>27</sup> and the noise in our data is much lower. The SH anomaly  $\Delta C/T|_{T_c}$  was estimated to be among 6~8 mJ/mol K<sup>2</sup>, being remarkably smaller than that of the FeAs-122 phase. Considering the formula based on the weak-coupling BCS theory  $\Delta C_e/\gamma_n T|_{T_c} = 1.43$ , we may evaluate the normal state electron SH coefficient  $\gamma_n \approx 4\text{--}6$  mJ/mol K<sup>2</sup>. We have known from Eq. (5) that  $\gamma_n$  is proportional to the normal state quasiparticle DOS  $N(E_F)$ . So the rather lower value of  $\gamma_n$  in the electron-doped  $\text{SmFeAsO}_{0.9}\text{F}_{0.1}$ , compared with that of the hole-doped  $\text{Ba}_{0.6}\text{K}_{0.4}\text{Fe}_2\text{As}_2$ , clearly illustrates that the normal state quasiparticle DOS in the electron-doped 1111 phase is remarkably lower than that in the holed-doped FeAs-122 system.

This large difference may be understood with the complex FS structures in the two systems. So far the ARPES data are consistent each other about the shape of the FSs around  $\Gamma$  point.<sup>20,23</sup> They also commonly point to a fact of s-wave gap on the FSs around  $\Gamma$ , given that the measurements about the gap symmetry were not influenced by the surface reconstruction. However there is a large difference between the results from different groups about the FSs around the M point.<sup>20,21,23</sup> It was reported that the FS near M point has a "propeller" shape with four elliptic blades surrounding a small circle FS.<sup>23</sup> How to understand this complex FS structure is very challenging. Concerning the pairing symmetry, one possibility is that there are nodes on these FSs near M point or at the positions of the connecting points of neighboring FSs. In the  $\text{Ba}_{0.6}\text{K}_{0.4}\text{Fe}_2\text{As}_2$  samples, the outer shell of the FSs surrounding  $\Gamma$  takes most of the weight and exhibits an full gap. While in the F-doped  $\text{LnFeAsO}$ , the

FSs near the M points become dominant and contribute more weight to the superfluid. This may explain why one can observe the nodal feature in the electron doped F-doped  $\text{LnFeAsO}$  samples in specific heat and point contact tunneling measurements.<sup>4,12</sup> Further momentum resolved experiments on  $\text{LnFeAsO}$  single crystals with good quality are highly desired to resolve this issue.

## VI. CONCLUDING REMARKS

In summary, the bulk evidence for the dominance of a full-gap superconducting state with the gap amplitude of about 6 meV was obtained in the hole-doped  $\text{Ba}_{0.6}\text{K}_{0.4}\text{Fe}_2\text{As}_2$  through low temperature SH measurements. An unexpected high SH anomaly  $\Delta C/T|_{T_c}$  and large value of  $\gamma_n$  were found, suggesting a very high normal state quasiparticle DOS. These two features make the present system very different from the FeAs-1111 phase. We also measured the SH of the high pressure synthesized electron-doped  $\text{SmFeAsO}_{0.9}\text{F}_{0.1}$ . It is found that  $\Delta C/T|_{T_c}$  and  $\gamma_n$  are only about a tenth of that of  $\text{Ba}_{0.6}\text{K}_{0.4}\text{Fe}_2\text{As}_2$ . We argue that this difference may be originated from the complex Fermi surface structures in different systems.

## Acknowledgments

We acknowledge the fruitful discussions with Tao Xiang, Fuchun Zhang, Huen-Dung Yang and Dung-Hai Lee. We also thank Prof. Zhongxian Zhao for providing the high-quality  $\text{SmFeAsO}_{0.9}\text{F}_{0.1}$  samples. This work is supported by the Natural Science Foundation of China, the Ministry of Science and Technology of China (973 project No: 2006CB601000, 2006CB921107, 2006CB921802), and Chinese Academy of Sciences (Project ITSNEM).

\* Electronic address: hhwen@aphy.iphy.ac.cn

<sup>1</sup> Y. Kamihara, T. Watanabe, M. Hirano, and H. Hosono, *J. Am. Chem. Soc.* **130**, 3296 (2008).

<sup>2</sup> H. H. Wen, G. Mu, L. Fang, H. Yang, and X. Y. Zhu, *Europhys. Lett.* **82**, 17009 (2008).

<sup>3</sup> M. Rotter, M. Tegel, and D. Johrendt, *Phys. Rev. Lett.* **101**, 107006 (2008). M. Rotter, M. Pangerl, M. Tegel, and D. Johrendt, *Angew. Chem. Int. Ed.* **47**, 7949 (2008).

<sup>4</sup> G. Mu, X. Y. Zhu, L. Fang, L. Shan, C. Ren, and H. H. Wen, *Chin. Phys. Lett.* **25**, 2221 (2008).

<sup>5</sup> H. Luetkens, H.-H. Klauss, R. Khasanov, A. Amato, R. Klingeler, I. Hellmann, N. Leps, A. Kondrat, C. Hess, A. Köhler, G. Behr, J. Werner, and B. Büchner, *Phys. Rev. Lett.* **101**, 097009 (2008).

<sup>6</sup> J. P. Carlo, Y. J. Uemura, T. Goko, G. J. MacDougall, J. A. Rodriguez, W. Yu, G. M. Luke, P. C. Dai, N. Shannon, S. Miyasaka, S. Suzuki, S. Tajima, G. F. Chen, W. Z. Hu,

J. L. Luo, and N. L. Wang, arXiv: cond-mat/0805.2186.

<sup>7</sup> A. J. Drew et al., arXiv: cond-mat/0805.2186.

<sup>8</sup> H. -J. Grafe, D. Paar, G. Lang, N. J. Curro, G. Behr, J. Werner, J. Hamann-Borrero, C. Hess, N. Leps, R. Klingeler, and B. Buechner, *Phys. Rev. Lett.* **101**, 047003 (2008).

<sup>9</sup> K. Matano, Z. A. Ren, X. L. Dong, L. L. Sun, Z. X. Zhao, and G. Q. Zheng, *Europhys. Lett.* **83**, 57001 (2008).

<sup>10</sup> K. Ahilan, F. L. Ning, T. Imai, A. S. Sefat, R. Jin, M. A. McGuire, B. C. Sales, and D. Mandrus, *Phys. Rev. B* **78**, 100501(R) (2008).

<sup>11</sup> C. Ren, Z. S. Wang, H. Yang, X. Y. Zhu, L. Fang, G. Mu, L. Shan, and H. H. Wen, arXiv: cond-mat/0804.1726.

<sup>12</sup> L. Shan, Y. L. Wang, X. Y. Zhu, G. Mu, L. Fang, C. Ren, and H. H. Wen, *Europhys. Lett.* **83**, 57004 (2008).

<sup>13</sup> T. Y. Chen, Z. Tesanovic, R. H. Liu, X. H. Chen, and C. L. Chien, *Nature* **453**, 1224 (2008).

<sup>14</sup> K. Hashimoto, T. Shibauchi, T. Kato, K. Ikada, R. Okazaki, H. Shishido, M. Ishikado, H. Kito, A. Iyo, H. Eisaki, S. Shamoto, and Y. Matsuda, arXiv: cond-mat/0806.3149.

<sup>15</sup> A. A. Aczel, E. Baggio-Saitovitch, S. L. Budko, P. C. Canfield, J. P. Carlo, G. F. Chen, P. C. Dai, T. Goko, W. Z. Hu, G. M. Luke, J. L. Luo, N. Ni, D. R. Sanchez-Candela, F. F. Tafti, N. L. Wang, T. J. Williams, W. Yu, and Y. J. Uemura, arXiv: cond-mat/0807.1044.

<sup>16</sup> C. Martin, R. T. Gordon, M. A. Tanatar, M. D. Vannette, M. E. Tillman, E. D. Mun, P. C. Canfield, V. G. Kogan, G. D. Samolyuk, J. Schmalian, and R. Prozorov, arXiv: cond-mat/0807.0876.

<sup>17</sup> L. Malone, J. D. Fletcher, A. Serafin, A. Carrington, N. D. Zhigadlo, Z. Bukowski, S. Katrych, and J. Karpinski, arXiv: cond-mat/0806.3908.

<sup>18</sup> X. Y. Zhu, H. Yang, L. Fang, G. Mu, and H. H. Wen, Supercond. Sci. Tech. **21**, 105001 (2008).

<sup>19</sup> H. Q. Luo, Z. S. Wang, H. Yang, P. Cheng, X. Y. Zhu, and H. H. Wen, Supercond. Sci. Technol. **21**, 125014 (2008).

<sup>20</sup> H. Ding, P. Richard, K. Nakayama, T. Sugawara, T. Arakane, Y. Sekiba, A. Takayama, S. Souma, T. Sato, T. Takahashi, Z. Wang, X. Dai, Z. Fang, G. F. Chen, J. L. Luo, and N. L. Wang, Europhys. Lett. **83**, 47001 (2008)..

<sup>21</sup> L. Zhao, H. Y. Liu, W. T. Zhang, J. Q. Meng, X. W. Jia, G. D. Liu, X. L. Dong, G. F. Chen, J. L. Luo, N. L. Wang, G. L. Wang, Y. Zhou, Y. Zhu, X. Y. Wang, Z. X. Zhao, Z. Y. Xu, C. T. Chen, and X. J. Zhou, Chin. Phys. Lett. **25**, 4402 (2008).

<sup>22</sup> L. Wray, D. Qian, D. Hsieh, Y. Xia, L. Li, J. G. Checkelsky, A. Pasupathy, K. K. Gomes, A. V. Fedorov, G. F. Chen, J. L. Luo, A. Yazdani, N. P. Ong, N. L. Wang, and M. Z. Hasan, arXiv: cond-mat/0808.2185.

<sup>23</sup> V. B. Zabolotnyy, D. S. Inosov, D. V. Evtushinsky, A. Koitzsch, A. A. Kordyuk, J. T. Park, D. Haug, V. Hinkov, A. V. Boris, D. L. Sun, G. L. Sun, C. T. Lin, B. Keimer, M. Knupfer, B. Buechner, A. Varykhalov, R. Follath, S. V. Borisenko, arXiv:cond-mat/0808.2454.

<sup>24</sup> N. R. Werthamer, E. Helfand, and P. C. Hohenberg, Phys. Rev. **147**, 295 (1966).

<sup>25</sup> Z. A. Ren, W. Lu, J. Yang, W. Yi, X. L. Shen, Z. C. Li, G. C. Che, X. L. Dong, L. L. Sun, F. Zhou, and Z. X. Zhao, Chin. Phys. Lett. **25**, 2215 (2008).

<sup>26</sup> A. S. Sefat, M. A. McGuire, B. C. Sales, R. Y. Jin, J. Y. Howe, and D. Mandrus, Phys. Rev. B **77**, 174503 (2008).

<sup>27</sup> L. Ding, C. He, J. K. Dong, T. Wu, R. H. Liu, X. H. Chen, and S. Y. Li, Phys. Rev. B **77**, 180510(R) (2008).

<sup>28</sup> Z. S. Wang, H. Q. Luo, C. Ren, H. H. Wen Phys. Rev. B **78**, 140501(R)(2008).

<sup>29</sup> H. M. Rosenberg, *Low Temperature Solid State Physics*, (Oxford University Press, Oxford, 1963).

<sup>30</sup> G. Mu, Y. Wang, L. Shan, and H. H. Wen, Phys. Rev. B **76**, 064527 (2007).

<sup>31</sup> K. Maki, in *Superconductivity*, edited by R. D. Parks (Marcel Dekker, New York, 1969), Vol. 2, p. 1035.

<sup>32</sup> N. E. Hussey, Adv. Phys. **51**, 1685 (2002)

<sup>33</sup> K. A. Moler, D. J. Baar, J. S. Urbach, R. X. Liang, W. N. Hardy, and A. Kapitulnik, Phys. Rev. Lett. **73**, 2744 (1994). K. A. Moler, J. R. Kirtley, R. X. Liang, D. Bonn, and W. N. Hardy , Phys. Rev. B **55**, 12753 (1997).

<sup>34</sup> B. Revaz, J. -Y. Genoud, A. Junod, K. Neumaier, A. Erb, and E. Walker, Phys. Rev. Lett. **80**, 3364 (1998).

<sup>35</sup> N. E. Phillips, R. A. Fisher, A. Schilling, B. Buffeteau, T. E. Hargreaves, C. Marcenat, R. Calemczuk, A. S. O'Connor, K. W. Dennis and R. W. McCallum, Physica B **259-261**, 546 (1999).

<sup>36</sup> H. H. Wen, Z. Y. Liu, F. Zhou, J. W. Xiong, W. X. Ti, T. Xiang, S. Komiya, X. F. Sun, and Y. Ando, Phys. Rev. B **70**, 214505 (2004). H. H. Wen, L. Shan, X. G. Wen, Y. Wang, H. Gao, Z. Y. Liu, F. Zhou, J. W. Xiong, and W. X. Ti, Phys. Rev. B **72**, 134507 (2005).

<sup>37</sup> S. H. Simon, and P. A. Lee, Phys. Rev. Lett. **78**, 1548 (1997).

<sup>38</sup> Z. Y. Liu, H. H. Wen, L. Shan, H. P. Yang, X. F. Lu, H. Gao, M. S. Park, C. U. Jung, and S. I. , Europhys. Lett. **69**, 263 (2005).

<sup>39</sup> D. J. Singh, Phys. Rev. B **78**, 094511 (2008).

<sup>40</sup> G. Xu, H. J. Zhang, X. Dai, and Z. Fang, arXiv:cond-mat/0807.1401.

<sup>41</sup> T. Yildirim, arXiv:cond-mat/0807.3936.

<sup>42</sup> F. J. Ma, Z. Y. Lu and T. Xiang, arXiv:cond-mat/0806.3526.

<sup>43</sup> I. R. Shein, and A. L. Ivanovskii, arXiv:cond-mat/0806.0750.